

Combatting noise in near-term quantum data centres

K. Campbell,* A. Lawey, and M. Razavi†

School of Electronic and Electrical Engineering, University of Leeds, Leeds, LS29JT, United Kingdom

We analyse the performance of different error handling methods in the quantum data centre paradigm of distributed quantum computing. We compare the impact of quantum error detection, using the three-qubit repetition code and the $[[4, 1, 2]]$ Leung-Nielsen-Chuang-Yamamoto code, on remote gates with that of conventional entanglement distillation techniques. Detailed classical simulation is used to obtain results for realistic near-term hardware.

I. INTRODUCTION

Distributed quantum computing is a promising strategy for scaling up quantum computers. By using a distributed architecture, it is possible to retain the high quality of local gates and physical qubits needed for fault-tolerant computing while circumventing the challenges associated with scaling up monolithic, single-processor, devices. However, new challenges arise in dealing with noisy entanglement between quantum processing units (QPUs) [1]. Previous work [1] indicates that entanglement errors dominate other forms of error, even when QPUs are in close proximity to each other, making entanglement errors a severe bottleneck to the feasibility of distributed quantum computing. In this work, we propose and evaluate various near-term strategies for mitigating the impact of entanglement noise over distributed quantum computers. Our focus will be on so-called quantum data centres (QDCs) [1], which have entangling connections between QPUs in the vicinity of each other.

A QDC consists of multiple spatially separated QPUs which each contain qubits and the control systems needed to apply unitary gate operations and measurements on them. QPUs are close enough together to share the same warehouse, with typical separations being of the order of metres or less. These QPUs are networked together to potentially enable larger scale computation.

Many of the challenges of implementing QDCs coalesce around one central issue: what happens when we wish to enact a two-qubit gate on qubits hosted by different QPUs? We call such a gate a remote gate. Remote gates involve several local, intra-QPU, operations, which will be imperfect and add noise to the system; classical communication, which adds latency; and, most damagingly of all [1], inter-QPU entanglement, or ebit, errors. Unmanaged, these errors severely inhibit the feasibility of QDCs [1] and so handling them is essential.

We consider two broad categories of error handling: quantum error detection (QED) and entanglement distillation, in the context of a remote CNOT gate. QED is closely related to the more powerful concept of quantum error correction [2], which can, in principle, eradicate errors from a quantum computer. However, the stringent requirements needed to implement enough fault-tolerant, error-corrected qubits of sufficient quality and quantity for useful applications exceed the capabilities of current hardware. It is far easier to detect errors and post-select results in which no errors are detected. It is also possible to do entanglement distillation, which uses local operations and classical communication to iteratively convert multiple noisy ebits into fewer, higher quality ebits [3, 4]. As with QED, entanglement distillation must be repeated until success and so has an associated time cost, leading to additional decoherence.

In our implementation of the remote CNOT gate using QED, instead of applying QED to ebits, we apply QED to the control qubit, in an arbitrary state, which we will then teleport. We encode the qubit's state in a stabiliser QED code [5] prior to teleportation and detect errors directly on the teleported state. In theory, our method has the advantage of also detecting errors caused by the local gates and measurements involved in the teleportation process but has the disadvantage that any detected errors require the entire algorithm in which the teleportation occurs to be restarted.

In contrast to much of the previous work on QED in the computing context [6–11], we do not assume (QED) encoding is retained throughout the entire algorithm, which would require many logical gates and qubits. Instead, we propose the localised application of QED to inter-QPU, or remote, gates, in which QED encoding is performed immediately prior to a remote gate and decoding is performed during the remote gate. The most similar work to ours is Ref. [12] but they consider detecting errors only on ebits and not the arbitrary unknown state of processing qubits.

For entanglement distillation, we extend previous work [13–15] by considering the average over all possible pure, separable input states to the remote gate, rather than assuming a known state is teleported. We also explicitly

* kennycampbell1@btinternet.com

† m.razavi@leeds.ac.uk

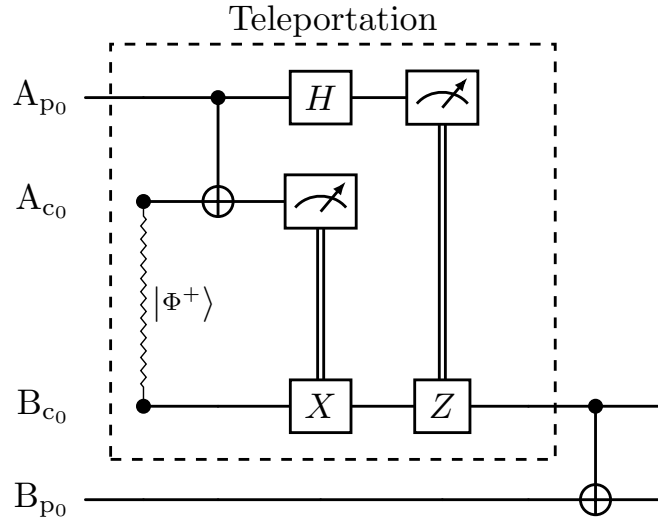


FIG. 1. A remote CNOT gate between qubits A_{p_0} and B_{p_0} implemented using the 1TP protocol. Zigzag lines indicate the distribution of an ebit, which, ideally, in the absence of noise, has the state $|\Phi^+\rangle = \frac{1}{\sqrt{2}}(|00\rangle + |11\rangle)$. Double lines indicate classical communication. The subscript c_i indicates a communication qubit with index i and p_i is a processing qubit with index i .

consider an entire remote CNOT gate rather than only the teleportation part [13, 14] or only the distribution of ebits [15]. This impacts the results if local errors are considered.

We make several additions to the existing literature. Our main contributions are as follows:

- We propose the notion of localised QED encoding as a means to improve the fidelity of remote gates in the QDC setting.
- We perform a circuit-level analysis of various QED schemes.
- We compare the relative performance of QED and entanglement distillation for near-term QDCs.

The remainder of the paper is structured as follows. In Sec. II, we introduce the schemes analysed in this paper. The error analysis conducted on these schemes is discussed in Sec. III. The results are then presented in Sec. IV. Finally, we conclude our discussion in Sec. V.

II. SYSTEM DESCRIPTION

As CNOT and single qubit gates are sufficient for universal quantum computing [5], we restrict ourselves to the study of remote CNOT gates for concreteness. We first consider the basic, unencoded remote gate in Sec. II A and then detail the additions that we make to it using QED, in Sec. II B, and entanglement distillation, in Sec. II C.

A. Unencoded case

We use a simple scheme, which we call 1TP [1], to implement remote gates, as shown in Fig. 1. To implement a 1TP remote CNOT, the control qubit, A_{p_0} , is teleported [16, 17] to B_{c_0} on the QPU containing the target qubit, B_{p_0} , and then the CNOT gate is conducted locally using B_{c_0} as the control qubit and B_{p_0} as the target qubit. Three different types of qubit are used: communication qubits, A_{c_0} and B_{c_0} , processing qubits, A_{p_0} and B_{p_0} , and flying qubits, which are not shown explicitly in Fig. 1. The flying qubits, which are typically photons, are used to distribute entanglement between the communication qubits on each QPU. The processing qubits, which may or may not be physically distinct from the communication qubits, are used much like qubits in a monolithic setting and do not interact directly with flying qubits.

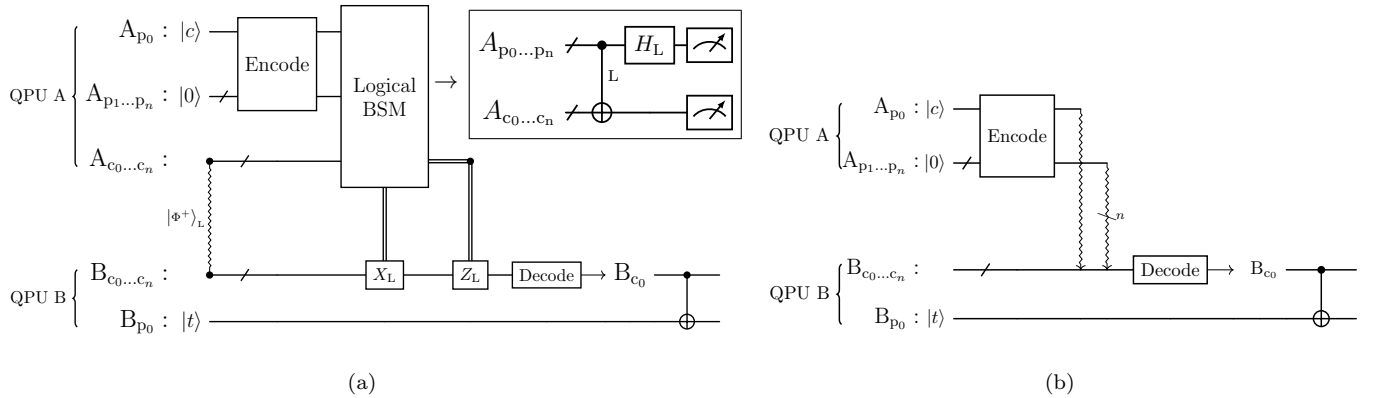


FIG. 2. 1TP remote CNOT gate using (a) fully-coded 1TP (FC-1TP) and (b) partially-coded 1TP (PC-1TP). The subscript L refers to a logical version of the operation or state. We omit the L for the measurements in (a) but both measurements are logical measurements. Double lines refer to classical communication, squiggly lines to the distribution of an ebit and squiggly arrows to quantum teleportations from the tail of the arrow to its head. $|c\rangle$ and $|t\rangle$ are arbitrary quantum states, which we assume to be separable from each other and pure in this work. If an error is detected during the decoding step then the final CNOT is not done and the entire process must be restarted.

B. QED schemes

We consider two broad ways of integrating QED into a 1TP remote CNOT gate, as shown in Fig. 2. The first scheme, shown in Fig. 2(a), is referred to as fully-coded 1TP (FC-1TP) and works as follows:

1. We first distribute a logical ebit, of the form $| \Phi^+ \rangle = \frac{1}{\sqrt{2}}(|00\rangle_L + |11\rangle_L)$, between both QPUs involved in the remote gate, where $|0\rangle_L$ and $|1\rangle_L$ are the logical computational basis eigenstates encoded in the QED code of choice. This is done, using the method discussed in Ref. [18] for encoded quantum repeaters, as follows:
 - (a) Qubits $A_{c_0 \dots c_n}$ are initially encoded in the logical state $|+\rangle_L = \frac{1}{\sqrt{2}}(|0\rangle_L + |1\rangle_L)$ and qubits $B_{c_0 \dots c_n}$ are encoded in the logical state $|0\rangle_L$.
 - (b) A logical remote CNOT gate is done between qubits $A_{c_0 \dots c_n}$ and $B_{c_0 \dots c_n}$. In our case, we only consider the repetition code for the first scheme and so $|0\rangle_L = |000\rangle$ and $|1\rangle_L = |111\rangle$ and the logical remote CNOT gate is done transversally using additional communication qubits, not shown in Fig. 2(a), to implement each of the physical remote gates. However, it is easy to generalise the same concepts to different QED codes.
2. Then, using $A_{p_1 \dots p_n}$, we apply local gates to encode qubit A_{p_0} .
3. After that, a logical BSM is applied, as shown in the box in the top-right corner of Fig. 2(a). Firstly, a logical CNOT is conducted between $A_{p_0 \dots p_n}$ and $A_{c_0 \dots c_n}$. Then, a logical X-basis measurement is done on $A_{p_0 \dots p_n}$ and a logical Z-basis measurement is done on $A_{c_0 \dots c_n}$.
4. The results of the measurements are sent from QPU A to QPU B and the local X and Z operations needed to complete the teleportation protocol are done on $B_{c_0 \dots c_n}$.
5. Finally, decoding is done and a physical CNOT gate is done between B_{c_0} and B_{p_0} . If errors are detected during decoding or the logical BSM, the CNOT gate is not done and the entire process is repeated from the beginning.

In the second scheme, shown in Fig. 2(b), logical ebots are not used. Instead, A_{p_0} is encoded into a QED code, using $A_{p_1 \dots p_n}$, as before, and then qubits $A_{p_0 \dots p_n}$ are individually teleported to $B_{c_0 \dots c_n}$, using additional ebots not shown in Fig. 2. After that, decoding is done, as in FC-1TP, and a local, unencoded, CNOT gate is done locally between B_{c_0} and B_{p_0} . We refer to this scheme as partially-coded 1TP (PC-1TP).

PC-1TP has the advantage of avoiding the need for any logical operations. This allows it to be used with a larger class of codes, such as the $[[4, 1, 2]]$ Leung-Nielsen-Chuang-Yamamoto (LNCY) code [19], for which not all of the logical gates needed for FC-1TP can be implemented transversally. For example, one can verify with manual calculation that, for the LNCY code, no transversal single-qubit logical Hadamard gate exists. PC-1TP is also trivial to extend to any other QED schemes without the need to worry about the fact that different QED codes use different logical gate implementations.

Figure 3 shows the encoding circuits for the specific codes used in this paper. Figure 3(a) encodes an arbitrary

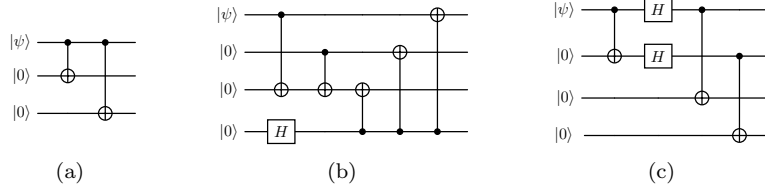


FIG. 3. Encoding circuits for (a) the three-qubit repetition code, (b) the Leung-Nielsen-Chuang-Yamamoto (LNCY) code [19] code using the encoder from [2], (c) a simpler encoding of the LNCY. $|\psi\rangle$ is an arbitrary quantum state.

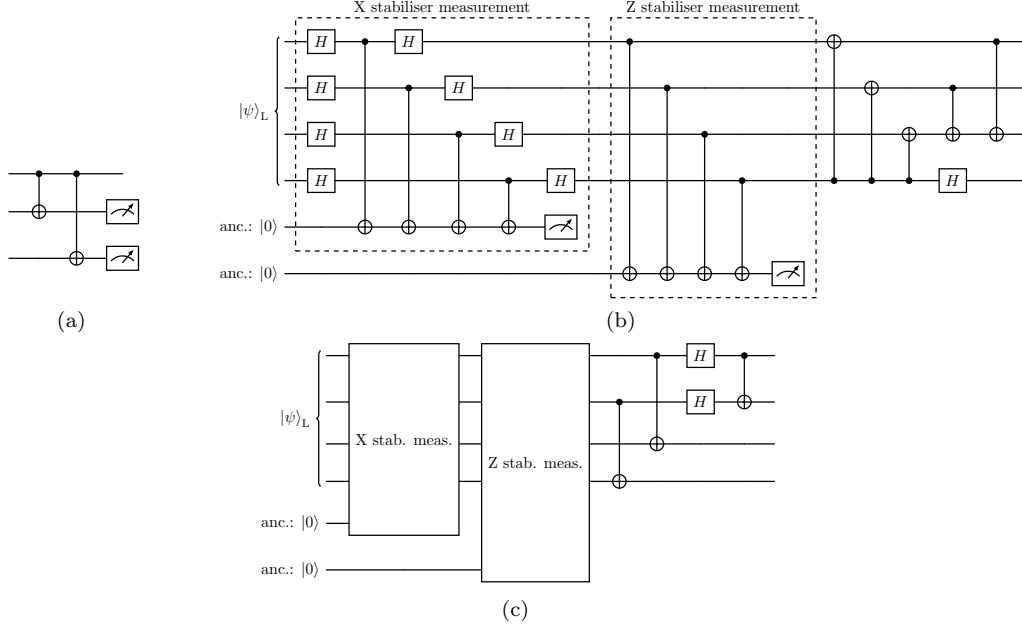


FIG. 4. Decoding/error detection circuits for (a) 3QRC, (b) 4QED, and (c) SS. The X and Z stabiliser measurements indicated in (c) are identical to those explicitly shown in (b). Qubits labelled ‘anc.’ are ancilla qubits. Everything after the Z stabiliser measurement in (b) and (c) is only done if no error was detected during the X and Z stabiliser measurements. If an error is detected, the result is discarded and the entire operation must be discarded.

quantum state into the three-qubit repetition code, which we shall refer to as 3QRC. This has the logical encoding $|0\rangle_L = |000\rangle$ and $|1\rangle_L = |111\rangle$ on the basis states. An arbitrary state, $|\psi\rangle = \alpha|0\rangle + \beta|1\rangle$, where $\alpha, \beta \in [0, 1]$ are normalised such that $|\alpha|^2 + |\beta|^2 = 1$, is encoded as $|\psi\rangle_L = \alpha|000\rangle + \beta|111\rangle$. We consider both FC-1TP and PC-1TP with 3QRC and refer to the former as FCRC and the latter as PCRC. Figs. 3(b) and 3(c) encode the $[[4, 1, 2]]$ LNCY [19], which, up to qubit relabelling, has the logical eigenstates $|0\rangle_L = \frac{1}{\sqrt{2}}(|0000\rangle + |1111\rangle)$ and $|1\rangle_L = \frac{1}{\sqrt{2}}(|0101\rangle + |1010\rangle)$. These are the $\{|00\rangle_L, |10\rangle_L\}$ logical basis states of the four-qubit code [8]. The encoding circuit shown in Fig. 3(c) is slightly more resource efficient, requiring fewer gates, but we include the encoding shown in Fig. 3(b) too, for the sake of comparison. We refer to the schemes shown in Figs. 3(b) and 3(c) as 4QED and SS, for shortened Shor¹, respectively. As previously discussed, it is challenging to implement FC-1TP for the LNCY code, and so we consider only PC-1TP for both 4QED and SS.

Unitary decoding of an arbitrary encoded state is done by running the encoding circuits in reverse². For the 3QRC decoder, we integrate error detection into the decoder similarly to the proposal in Ref. [21]. For 4QED and SS, we instead detect errors prior to decoding using a stabiliser measurement [2] and then run the unitary decoding circuits. This requires the use of additional, ancilla qubits. The decoding/error detecting circuits used are shown in Fig. 4. The X stabiliser measurements in Figs. 4(b) and 4(c) detect Z errors and the Z stabiliser measurements detect X errors [2, 5].

¹ Both of the $[[4, 1, 2]]$ codes used are equivalent if one of the qubits in the first scheme is used as a gauge qubit, meaning it is essentially ignored, and both codes can be thought of as a shortened version of the Shor code [20], but, in the interests of telling them apart, we attach this name only to one of the codes.

² If the encoding gates all commute, as they do for 3QRC, then the encoding circuit can be used unchanged.

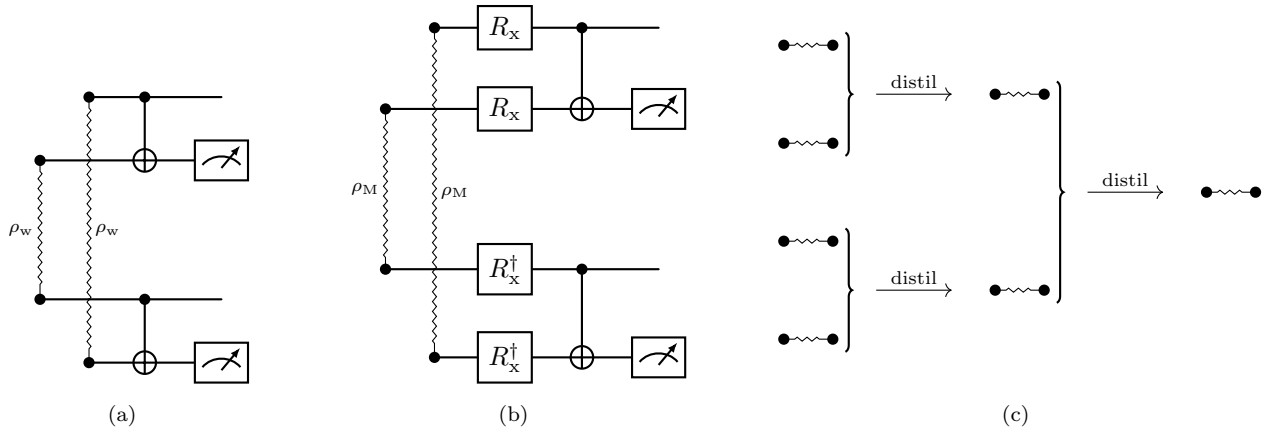


FIG. 5. The (a) BBPSSW, (b) DEJMPS and (c) general two-round entanglement distillation schemes. BBPSSW assumes a Werner state input, which can be enforced with local operations, although this is not done here, while DEJMPS allows a more general input. For both schemes, the circuit is run repeatedly until both of the measurements shown give the same result. The squiggly lines indicate the distribution of the state $|\Phi^+\rangle = \frac{1}{\sqrt{2}}(|00\rangle + |11\rangle)$, in the ideal case where no noise is present. In reality, noise will be present and for BBPSSW, it is assumed that this noise has the Werner form, as discussed in the main text. For DEJMPS, no such assumptions are made and the state ρ_M can instead be distributed, which is an arbitrary mixture of the different Bell states $|\Phi^\pm\rangle = \frac{1}{\sqrt{2}}(|00\rangle \pm |11\rangle)$, $|\Psi^\pm\rangle = \frac{1}{\sqrt{2}}(|01\rangle \pm |10\rangle)$. R_x is a $\frac{\pi}{2}$ rotation about the x axis and R_x^\dagger is the $-\frac{\pi}{2}$ rotation. (a) and (b) show just one round of entanglement distillation here, but the fidelity can be further improved by further distilling the outcome as illustrated in (c).

C. Entanglement distillation schemes

To implement a remote CNOT gate with entanglement distillation, we use the unencoded scheme shown in Fig. 1 but apply entanglement distillation to the ebits. Two entanglement distillation schemes are considered, the scheme proposed in Ref. [3], termed BBPSSW, and that of Ref. [4], termed DEJMPS, hereafter. The schemes are shown in Figs. 5(a) and 5(b), respectively. The schemes differ primarily in the assumptions that they make about the initial entangled state. BBPSSW is conducted by first distributing two ebits, which are assumed to be in the Werner state, defined as follows:

$$\rho_W = F_W |\Phi^+\rangle\langle\Phi^+| + \frac{1-F_W}{3} (|\Phi^-\rangle\langle\Phi^-| + |\Psi^+\rangle\langle\Psi^+| + |\Psi^-\rangle\langle\Psi^-|), \quad (1)$$

where $F_W \in [0, 1]$, $|\Phi^\pm\rangle = \frac{1}{\sqrt{2}}(|00\rangle \pm |11\rangle)$, and $|\Psi^\pm\rangle = \frac{1}{\sqrt{2}}(|01\rangle \pm |10\rangle)$. This assumption can be enforced using random single-qubit gates [3], but, in this work, we assume that the state of the initial ebit already has the above form, as we consistently use the Werner state to model entanglement noise throughout this work. BBPSSW also requires $F_W \geq 0.5$.

The second scheme, DEJMPS, instead assumes that the ebits have the more general state

$$\rho_M = A|\Phi^+\rangle\langle\Phi^+| + B|\Psi^-\rangle\langle\Psi^-| + C|\Psi^+\rangle\langle\Psi^+| + D|\Phi^-\rangle\langle\Phi^-|, \quad (2)$$

where $A, B, C, D \in [0, 1]$, $A + B + C + D = 1$, and $A \geq 0.5$. However, for consistency with our error analysis of the QED schemes, we again assume that the initial, pre-distillation ebits have the Werner state in Eq. (1).

After the entanglement distribution step, DEJMPS applies the operation $R_X \otimes R_X^\dagger$, to each ebit, where R_X is a $+\frac{\pi}{2}$ rotation about the x axis. This swaps B and D in Eq. (2). After that, the same local operations and measurements as BBPSSW are used.

Both schemes start with two pairs of entangled states entangled between two QPUs, apply CNOT gates locally on their share of the entangled states, and then measure the target qubits. The measurement results are compared and if they do not have the same value then the unmeasured qubits are discarded. This process distinguishes between the $|\Phi^\pm\rangle$ and $|\Psi^\pm\rangle$ states [3]. The entire process is repeated until both measurement results are the same.

It is possible to improve the fidelity by nesting the entanglement distillation process so that already distilled ebits are distilled again. This is shown in Fig. 5(c). DEJMPS is known to perform better than BBPSSW when multiple nested rounds of entanglement distillation are done [4] and so we consider nesting only for DEJMPS. In the nested DEJMPS protocol, four ebits are initially distributed sequentially, waiting for one distribution to finish before starting

the next³. Then, they are distilled into two higher-fidelity ebits. Those two distilled ebits are then distilled again to make a single ebit. If either distillation fails, we repeat the entire process again, creating four ebits and distilling them until the entire protocol succeeds⁴. We refer to this nested protocol as DEJMP4 to distinguish it from the single-round case where we start with two ebits and distill them into a single ebit, which we call DEJMP2.

III. ERROR ANALYSIS

We subject the various implementations of a remote CNOT gate discussed in Sec. II to various types of error. We do this using discrete event simulation, which is discussed in Sec. III A. The noise models used are discussed in Sec. III B. We also calculate the success rates of the different implementations, as discussed in Sec. III C.

A. Discrete event simulation

The majority of the results in this work are taken using discrete event simulation with NetSquid [22] and the related dqc_simulator package we developed [23]. This means that time, t , does not progress continuously but is instead a discrete variable, which increases in increments only when something, an event, happens. For example, a classical message arriving at the receiver would be an event and only when the message arrives would we apply the memory decoherence accrued when waiting for that message. All classical and quantum operations we consider have an associated duration, and when the operation finishes, we increment t by that amount. Some operations also have associated noise models, which are implemented using quantum channels. Further details on the channels used are provided in Sec. III B. The quantum state of the system is tracked by grouping together all qubits that are entangled with each other and tracking the density matrix for each group of qubits after a given event, re-assigning qubits to new groups to represent changes in entanglement, where appropriate.

Some abstractions and constraints are used for convenience of simulation. Firstly, ebits are generated at a black box central source in the Werner state, given by Eq. (1) and the constituent qubits travel to the QPUs. Upon arrival, the qubits are treated as communication qubits and we do not explicitly model the transduction between communication qubits and photons. The noise generated by the various subprocesses that would occur in real experiments is amalgamated into Eq. (1). Similarly, the latency of the entire process is amalgamated into a single parameter, t_{dist} , representing the entanglement distribution time. Secondly, the remote gates or individual teleportations used by the FC-1TP and PC-1TP, respectively are done sequentially, due to limitations on the simple scheduler used. For both entanglement distillation schemes, ebit distribution is again done sequentially. With more advanced scheduling, parallelisation would be possible for ebit distribution, remote gates and teleportations. Finally, we neglect the classical processing time needed for classical logic. For example, the time taken to interpret classical messages or recognise that ebits have arrived at a QPU is neglected.

B. Noise models

In addition to the initial ebit noise modelled by Eq. (1), we model other sources of noise in our system using several variants of the depolarising noise channel [5]. First, consider single-qubit gates. For a multi-qubit system in state ρ_{in} , acting the unitary operation U_i on qubit i results in the following transformation:

$$\rho_{\text{in}} \rightarrow (1 - \epsilon_{\text{sg}})U_i\rho_{\text{in}}U_i^\dagger + \frac{\epsilon_{\text{sg}}}{2}\text{Tr}_i(\rho_{\text{in}}) \otimes \mathbb{1}_i, \quad (3)$$

where ϵ_{sg} is the probability of error occurring for single-qubit gates, Tr_i is the partial trace with respect to qubit i , and $\mathbb{1}_i$ is its corresponding identity matrix.

For a two-qubit gate, $U_{i,j}$, acting on qubits i and j , the channel has the following form [24]:

$$\rho_{\text{in}} \rightarrow (1 - \epsilon_{\text{tg}})U_{i,j}\rho_{\text{in}}U_{i,j}^\dagger + \frac{\epsilon_{\text{tg}}}{4}\text{Tr}_{i,j}(\rho_{\text{in}}) \otimes \mathbb{1}_{i,j}, \quad (4)$$

where ϵ_{tg} is the probability of error for two-qubit gates, $\text{Tr}_{i,j}$ is the partial trace over qubits i and j , and $\mathbb{1}_{i,j}$ is the identity matrix on i and j .

³ This is not optimal. Clearly, parallelisation could be done here, however for ease of simulation, we have not done so.

⁴ If one of the distillations is successful and the other fails, we could retain the successfully distilled ebit and discard only the unsuccessfully distilled one. This would arguably be more efficient but risks memory decoherence damaging the previously distilled ebit while it waits for another ebit to be successfully distilled. To avoid such complications, we discard both pairs but note that this may be sub-optimal.

We also consider memory depolarisation, which is acted on qubits individually as time passes. This is done using the channel

$$\rho_{\text{in}} \rightarrow e^{-\Delta t r} \rho_{\text{in}} + \frac{(1 - e^{-\Delta t r})}{3} (X_i \rho_{\text{in}} X_i + Y_i \rho_{\text{in}} Y_i + Z_i \rho_{\text{in}} Z_i), \quad (5)$$

where i is the qubit being acted on; Δt is the time since the last event; X_i , Y_i , and Z_i are the Pauli operations acting on qubit i ; and r is the memory depolarisation rate, which is a parameter of the hardware.

As detailed in Sec. III A, we use event-based simulation, and so any physical process, such as a gate or the sending of a classical message has an associated duration. After each event, we apply Eq. (5) to all relevant qubits.

Finally, we impose errors during Z-basis measurements⁵ on qubit i using the bit-flip channel:

$$\rho_{\text{in}} \rightarrow (1 - \epsilon_m) \rho_{\text{in}} + \epsilon_m X_i \rho_{\text{in}} X_i, \quad (6)$$

where ϵ_m is the probability of a measurement error.

C. Success probability

As well as the noise modelled in the previous section, there is also an associated latency cost to QED and entanglement distillation. To indirectly evaluate this, we calculate the success probability, p_s , of a given attempt of the DEJMPS or 4QED/SS protocols as a function of F_w . For simplicity, we ignore other sources of error in this section.

For DEJMPS, the following expression is provided in Ref. [4]:

$$p_s = (A + B)^2 + (C + D)^2. \quad (7)$$

For multiple rounds of DEJMPS, we must recursively update the values of A , B , C and D in Eq. (7). We do this using the the following expressions from Ref. [4]:

$$\begin{aligned} \tilde{A} &= \frac{A^2 + B^2}{p_s}, \\ \tilde{B} &= \frac{2CD}{p_s}, \\ \tilde{C} &= \frac{C^2 + D^2}{p_s}, \\ \tilde{D} &= \frac{2AB}{p_s}, \end{aligned} \quad (8)$$

where \tilde{A} to \tilde{D} are the average post-distillation values of A to D .

For 4QED/SS, we find

$$p_s = F_w^4 + \frac{(1 - F_w)^4}{27} + 2F_w^2(1 - F_w)^2, \quad (9)$$

through exhaustive consideration of the all scenarios in which no error occurs or errors that occur remain undetected; see Appendix A. The latter stipulation is important and applies to DEJMPS as well. Errors can occur in a “successful” entanglement distillation or error detection process. For 4QED/SS, undetected errors are caused by even numbers of the same type of error, as in such cases, the parity with respect to the relevant error type is unchanged and so the stabiliser measurement results are indistinguishable from when no error had occurred.

IV. NUMERICAL RESULTS

We evaluate the performance of the schemes introduced in Sec. II using a classical, event-based simulator that we built in Python 3.9 using the NetSquid library [22] and the related dqc_simulator package that we wrote [23], see Sec.

⁵ We construct any X-basis measurements using a Hadamard followed by a Z-basis measurement, so all of our measurements are Z-basis measurements.

TABLE I. The durations of all operations considered.

Parameter	Value	Source
Single-qubit gate time	$135\ \mu\text{s}$	[25]
Two-qubit gate time	$600\ \mu\text{s}$	[25]
Measurement time	6 ms	Inferred from [25–27]
Classical comm. time	$10^{-8}\ \text{s}$	[28, 29]
Ebit. distr. time	$\frac{1}{182}\ \text{s}$	[28]

TABLE II. The percentage difference between the minimum and maximum values of F_{out} , $\Delta_{\text{mm}} = \frac{(F_{\text{out}})_{\text{max}} - (F_{\text{out}})_{\text{min}}}{(F_{\text{out}})_{\text{min}}} \times 100$, where $(F_{\text{out}})_{\text{max}}$ and $(F_{\text{out}})_{\text{min}}$ are the maximum and minimum values of F_{out} , respectively, and all noise parameters are fixed, so that only the input state of the control and target qubits is varied. The minimum and maximum values of Δ_{mm} shown are obtained when $F_w = 0.99$ and $F_w = 0.9$, respectively.

Parameter set	Scheme	Min. Δ_{mm} (%)	Max. Δ_{mm} (%)
1	BBPSSW	0.671	7.10
1	DEJMPS4	4.51×10^{-3}	0.507
1	4QED	4.51×10^{-3}	0.504
1	SS	4.51×10^{-3}	0.504
1	FCRC	1.01	11.0
1	PCRC	1.01	11.0
2	BBPSSW	1.02	7.09
2	DEJMPS2	1.09	7.53
2	DEJMPS4	0.71	2.12
2	4QED	0.277	0.886
2	SS	0.121	0.737

III A. All simulations were run on a high-end desktop computer with a 2.5 GHz 11th generation Intel core i7-11700 processor and 32 GB of RAM. The primary figure of merit considered is the fidelity, F_{out} , of the output state from the remote gate, relative to the ideal output state in the absence of noise.

The values we use for the durations of different operations, and their corresponding references, are listed in Table I. The single-qubit gate time and two-qubit gate time used are sampled from the specifications for IonQ Aria [25], a commercial trapped-ion device. The measurement time is estimated from the two-qubit gate time, based on the assertion made in Refs. [26, 27] that the measurement time is five to ten times larger than the two-qubit gate time for trapped-ion quantum computers. We therefore choose the measurement time to be ten times the two-qubit gate time used. The classical communication time is taken to be the time to cross an optical fibre at $2 \times 10^8\ \text{ms}^{-1}$ [29]⁶. This neglects any classical processing times but gives a rough estimate of the classical communication times. For the ebit distribution time, t_{dist} , we use $t_{\text{dist}} = \frac{1}{R_{\text{dist}}}$, where $R_{\text{dist}} = 182\ \text{Hz}$ is the average entanglement distillation rate found in Ref. [28].

Based on our discrete-event simulations, we find that the output fidelity of the schemes introduced in Sec. II depends on their input states. To see this, we consider the percentage difference between the minimum, $(F_{\text{out}})_{\text{min}}$, and maximum, $(F_{\text{out}})_{\text{max}}$, values of F_{out} , $\Delta_{\text{mm}} = \frac{(F_{\text{out}})_{\text{max}} - (F_{\text{out}})_{\text{min}}}{(F_{\text{out}})_{\text{min}}} \times 100$. When computing Δ_{mm} , all parameters are fixed other than the input states of the control and target qubits, which are both uniformly sampled from the Bloch sphere. We consider 40,000 data points when computing each of the Δ_{mm} values and tabulate the results in Table II. In particular, Table II shows the maximum and minimum values of Δ_{mm} for parameter sets 1 and 2, which correspond to $F_w \in [0.90, 0.99]$, $\epsilon_{\text{sg}} = \epsilon_{\text{tg}} = \epsilon_{\text{m}} = r = 0$; and $F_w \in [0.90, 0.99]$, $\epsilon_{\text{sg}} = 1.8 \times 10^{-5}$, $\epsilon_{\text{tg}} = 9.7 \times 10^{-4}$, $\epsilon_{\text{m}} = 2.33 \times 10^{-3}$, $r = 0.055\ \text{Hz}$, respectively. The fixed, local error parameters from parameter set 2 are based on those used by real hardware. For everything except r , the values for Quantinuum's H1 processor [30] are used. For r , the midpoint of the quoted range for $\frac{1}{T_1}$ is used with T_1 taken from the data for IonQ Aria [25]. The parameters from the H1 and IonQ Aria machines are used because they represent the approximate state of the art for these parameters on commercial hardware at the time of writing⁷. In each case, the minimum value of Δ_{mm} is given by $F_w = 0.99$ and the maximum value occurs when $F_w = 0.9$.

⁶ Ref. [29] quotes the speed as a refractive index but the speed, v , of light in the fibre is easily inferable using the formula $v = \frac{c}{n}$ where c is the speed of light in vacuum and n is the refractive index. The formula follows from the definition of refractive index $n = \frac{c}{v}$.

⁷ Both Quantinuum and IonQ have released newer devices with additional qubits and features, but the parameters that I am considering are similar or slightly better for H1 and Aria at the time of running our simulations.

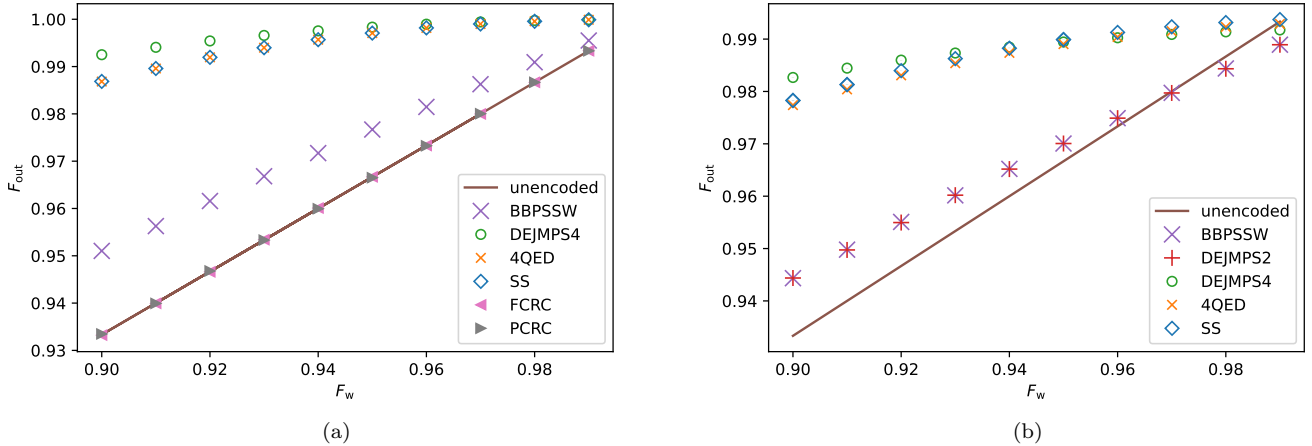


FIG. 6. \bar{F}_{out} , averaged over all possible pure, separable input states to a remote CNOT gate as a function of F_w for (a) $\epsilon_{\text{sg}} = \epsilon_{\text{tg}} = \epsilon_{\text{m}} = r = 0$, (b) $\epsilon_{\text{sg}} = 1.8 \times 10^{-5}$, $\epsilon_{\text{tg}} = 9.7 \times 10^{-4}$, $\epsilon_{\text{m}} = 2.33 \times 10^{-3}$ and $r = 0.055\text{Hz}$. Each data point is averaged over 40,000 F_{out} values generated with different input states uniformly sampled from the Bloch sphere of the control and target qubits. The different curves represent the results for the different error mitigation schemes considered in Secs. II B and II C. As discussed in the main text, BBPSSW and DEJMPS are the entanglement distribution schemes from Refs. [3] and [4], respectively; DEJMPS2 is two-ebit DEJMPS; DEJMPS4 is four-ebit DEJMPS; 4QED and SS are the LNCY [19] code implemented using Fig. 3(b) and Fig. 3(c), respectively. Error bars show the standard error, which is too small to be visible here.

From Table 2 we can see that altering the input state can produce percentage differences as large as $\Delta_{\text{mm}} = 11.0\%$ for some error handling schemes when $F_w = 0.9\%$ and the percentage difference can still reach up to $\Delta_{\text{mm}} = 1.09\%$ when $F_w = 0.99$ for DEJMPS2. As such, it is clearly important to account for the role played by the input state, especially when the entanglement error is high. The input state to a given remote gate within a distributed circuit will not generally be known, so we consider the average over all pure, separable input states. The assumption of pure, separable input states limits the applicability of our findings to remote gates for which the control and target qubits are not initially entangled with any other qubits or each other, but greatly simplifies the problem. Averaging is done by the Monte Carlo method with uniform sampling of the input states of the control and target qubits from the Bloch sphere. 40,000 data points are taken for each average value computed. We denote the average output fidelity over such input states as \bar{F}_{out} .

To obtain an upper bound on performance, we first consider how each scheme performs in the presence of entanglement errors only. We consider the parameters $F_w \in [0.90, 0.99]$, $\epsilon_{\text{sg}} = \epsilon_{\text{tg}} = \epsilon_{\text{m}} = r = 0$, and plot \bar{F}_{out} as a function of F_w . The results of this analysis are shown in Fig. 6(a). From Fig. 6(a), the following observations can be made:

1. The repetition code schemes, FCRC and PCRC, are indistinguishable from each other in the presence of entanglement error. It is interesting that there is no intrinsic entanglement error reduction benefit to using the more complicated FCRC scheme over the simpler PCRC scheme in our scenario. The PC-1TP method, shown in Fig. 2, benefits from a reduced gate count, greater simplicity and easier generalisation to other QED codes. For this reason, we use this scheme for the remaining codes investigated.
2. Even in the absence of local errors, neither FCRC or PCRC shows any benefit, on average, over the unencoded remote gate. From inspection of the data, significant advantage is found over the unencoded case for certain input states but for others they actually do worse than the unencoded case. This is mainly due to the fact that the repetition code used detects bit flip errors as opposed to phase flip ones. More details on this are provided in Appendix B. However, we have been unable to infer a clear pattern as to which input states do better than others.
3. Entanglement distillation and both four-qubit error detection schemes, 4QED and SS, all provide a clear advantage over the unencoded case. The greatest advantage is provided by DEJMPS4 followed by 4QED and SS, with the least advantage offered by BBPSSW. It can be verified analytically that DEJMPS2 yields an identical entanglement fidelity to BBPSSW in this scenario and so is not shown.
4. 4QED and SS give essentially identical results. The difference between any two results always falls within the

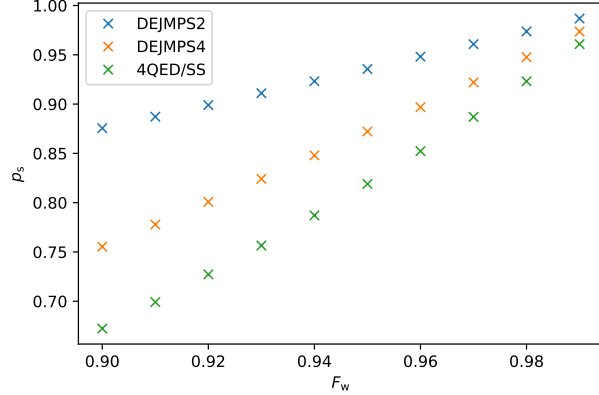


FIG. 7. Success probability for different error mitigation schemes with varying F_w and $\epsilon_{sg} = \epsilon_{tg} = \epsilon_m = r = 0$.

standard error range of the results. This is to be expected, as in the absence of local errors, there is very little to distinguish the encoders and decoders of the two schemes.

We also consider the more realistic setting where finite local errors are present in the circuit. We use the parameters $F_w \in [0.90, 0.99]$, $\epsilon_{sg} = 1.8 \times 10^{-5}$, $\epsilon_{tg} = 9.7 \times 10^{-4}$, $\epsilon_m = 2.33 \times 10^{-3}$ and $r = 0.055$ Hz. Again, \bar{F}_{out} is plotted for F_w in the previously stated range to produce Fig. 6(b). Based on Fig. 6(b), we observe:

1. As was the case previously, both of the four-qubit QED schemes considered, 4QED and SS, outperform both two-ebit entanglement distillation schemes. DEJMPS4, however, does a little better than 4QED and SS for $F_w < 0.95$ and very slightly worse thereafter. The discrepancy between DEJMPS4 and 4QED/SS is always small for all considered F_w values.
2. 4QED, SS and DEJMPS4 have a very clear advantage over the unencoded case until around $F_w = 0.99$, at which point they perform similarly to the unencoded case. Therefore, there is a clear benefit to their use with current or near-term hardware.
3. DEJMPS2 and BBPSSW are almost identical, with at most 0.01% between them and neither scheme being consistently better for all F_w .
4. BBPSSW and DEJMPS2 outperform the unencoded case for $F_w \lesssim 0.97$ but offer a much smaller advantage than the DEJMPS4, 4QED and SS.
5. SS slightly outperforms 4QED in the presence of the local error values considered, but the discrepancy between the two schemes remains very low. Overall, it seems that the slightly less gate efficient encoder and decoder used in 4QED makes very little difference in this scenario because the magnitude of the local errors are too low for a few gates to have a significant impact.

From the \bar{F}_{out} results alone there is little to distinguish between 4QED/SS, which are similar enough to be discussed together here, and DEJMPS4. However, there are other practical considerations to consider. The first of these is that 4QED/SS requires more qubits to implement than DEJMPS4, as both schemes need four communication qubits available but 4QED/SS requires an additional three processing qubits on one QPU, with which to encode the control qubit prior to teleportation.

Another area in which there is some distinction is the impact of each scheme on the latency. A key facet of this is the fact that failed rounds of DEJMPS only require communication qubits to be discarded and so do not destroy any quantum information required to complete the algorithm, which is stored in the processing qubits. The ebits used in DEJMPS are a consumable resource and the only cost to discarding them is time. By contrast, if 4QED/SS fails then the entire algorithm must be restarted as there is a detected error in the processing qubits. Therefore, if the success probability, p_s , of 4QED/SS and DEJMPS is comparable then the latency cost of 4QED/SS will be much higher for larger circuits.

Using Eqs. (7) and (9), we find that DEJMPS actually has a higher p_s than 4QED/SS, with DEJMPS2 being up to 30.2% greater than 4QED and DEJMPS4 being up to 12.4% greater. We plot p_s as a function of F_w , with $\epsilon_{sg} = \epsilon_{tg} = \epsilon_m = r = 0$, in Fig. 7. From Fig. 7, we can see that, for all F_w values, p_s is highest for DEJMPS2, followed

by DEJMPS4 with 4QED/SS having the lowest rate. As such, in the particular case considered here, entanglement distillation introduces a lower latency than localised QED encoding. That said, QED schemes provide a pathway solution between the current state of the art, with no encoding, and the eventual fault-tolerant schemes. As such, their analysis and implementation could offer hints on how to move forward.

V. CONCLUSION

In this work, we applied quantum error detection to remote gates as a means of improving fidelity and investigated the performance of those schemes and entanglement distillation in increasing the fidelity of remote gates within the quantum data centre context. Taken together, our results suggest that, of the error mitigation schemes considered, entanglement distillation is most suitable for use in resource-constrained, near-term applications, as entanglement distillation is able to improve the average output fidelity better or comparably to the error detection schemes investigated, with fewer qubits and a lower latency cost. For the former, an alternative, not considered in this work, would be to perform error detection only on the ebit resources and decode prior to beginning teleportation, which may offer better performance. That solution is conceptually very similar to entanglement distillation.

There is a trade-off between the better fidelity improvement of four-ebit, two-round DEJMPS entanglement distillation and the faster implementation and lower qubit cost of two-ebit, one-round DEJMPS. However, the significant improvement in output fidelity of four-ebit DEJMPS relative to two-ebit DEJMPS most likely makes it worth doing at least two rounds of entanglement distillation.

The [[4, 1, 2]] LNCY [19] also shows a clear improvement over the unencoded case and future investigation of alternative error detection codes or optimisations is merited. However, the three-qubit repetition code is unlikely to be useful for quantum computing purposes in the quantum data centre context.

Appendix A: Analytical calculations of success probability

The success probability, p_s , of 4QED/SS is provided in Eq. (9) of the main text. Here, we derive Eq. (9).

We assume that only entanglement errors are present and that all ebits used during teleportation have the form given in Eq. (1). After teleportation of the encoded qubit, but prior to decoding, we obtain the state

$$\rho_t = \sum_{i=1}^4 \sum_{j=1}^4 \sum_{k=1}^4 \sum_{l=1}^4 p_{ijkl} R_{ijkl} \rho_{\text{ideal}} R_{ijkl}^\dagger, \quad (\text{A1})$$

where $R_{ijkl} = R_i \otimes R_j \otimes R_k \otimes R_l$ for $R_i \in \{\mathbb{1}, X, Z, XZ\}$ and $i, j, k, l \in \{1, 2, 3, 4\}$, p_{ijkl} is the probability of error R_{ijkl} occurring, and ρ_{ideal} is the ideal teleported state.

Of all the summands, only those for which no error occurs, or errors occur but remain undetected, count towards the success probability. Only one term in Eq. (A1) has no errors and this occurs with probability

$$p_0 = F_w^4. \quad (\text{A2})$$

Undetected errors occur when there are an even number of the same type of errors, meaning that the stabiliser measurements remain unchanged from the no error case. This means that there are either two or four different errors on different qubits.

For the two-error case, there are 18 ways in which this can occur, each occurring with probability

$$F_w^2 \left(\frac{1 - F_w}{3} \right)^2.$$

As such the probability of having exactly two errors, p_2 , is

$$p_2 = 18 \times F_w^2 \left(\frac{1 - F_w}{3} \right)^2 = 2F_w^2(1 - F_w)^2. \quad (\text{A3})$$

A similar process yields a four error probability, p_4 , of

$$p_4 = \frac{(1 - F_w)^4}{27}. \quad (\text{A4})$$

Adding the right-hand sides of Eqs. (A2), (A3), and (A4) will give us Eq. 9 in the main text.

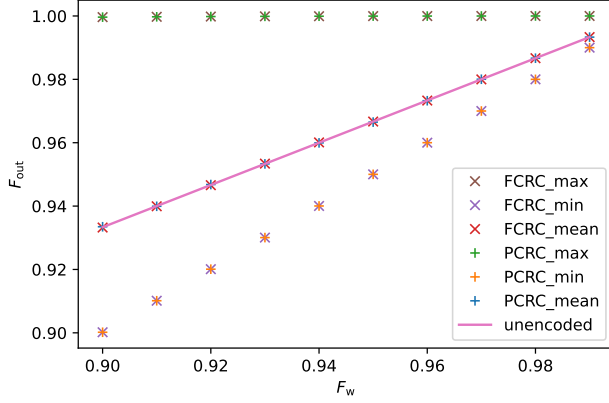


FIG. 8. The min, max and mean F_{out} with respect to the parameters $F_w \in [0.90, 0.99]$, $\epsilon_{\text{sg}} = \epsilon_{\text{tg}} = \epsilon_{\text{m}} = r = 0$, for a remote CNOT gate encoded using FCRC and PCRC.

Appendix B: Input states and the repetition code performance

In the second observation on Fig. 6(a) that we make in Sec. IV, we note that neither FCRC nor PCRC shows any benefit on average over the unencoded case, but there is a significant advantage to using FCRC/PCRC for some input states and a disadvantage in other cases. Here, we expand upon that statement.

Figure 8 shows the minimum, maximum and mean values of F_{out} for a remote CNOT gate implemented using FCRC and PCRC. The parameters are $F_w \in [0.90, 0.99]$, $\epsilon_{\text{sg}} = \epsilon_{\text{tg}} = \epsilon_{\text{m}} = r = 0$. For each datapoint, the result is sampled from 40,000 raw data points for which no error was detected. From Fig. 8, we can see that for some input states, both FCRC and PCRC correct almost all of the error. However, for other input states, the encoded case actually does worse than the unencoded case, even in the absence of local errors. In such scenarios, it seems that the additional phase errors imposed on the system by using additional imperfect ebits, counteracts any benefit to the repetition code error detection, which detects only bit flips. These effects balance out on average to confer no benefit relative to the unencoded case.

The natural next question to ask is for which input states is F_{out} better and worse than the unencoded case but there does not seem to be a discernible pattern to this behaviour and so we can only conclude that the results vary greatly with the input state.

[1] K. Campbell, A. Lawey, and M. Razavi, Quantum data centres: a simulation-based comparative noise analysis, *Quantum Science and Technology* **10**, 015052 (2024).

[2] J. Roffe, Quantum error correction: An introductory guide, *Contemporary Physics* **60**, 226 (2019).

[3] C. H. Bennett, G. Brassard, S. Popescu, B. Schumacher, J. A. Smolin, and W. K. Wootters, Purification of noisy entanglement and faithful teleportation via noisy channels, *Physical Review Letters* **76**, 722 (1996).

[4] D. Deutsch, A. Ekert, R. Jozsa, C. Macchiavello, S. Popescu, and A. Sanpera, Quantum privacy amplification and the security of quantum cryptography over noisy channels, *Physical Review Letters* **77**, 2818 (1996).

[5] M. Nielsen and I. Chuang, *Quantum Computation and Quantum Information*, 10th ed. (Cambridge University Press, 2010).

[6] D. Gottesman, Quantum fault tolerance in small experiments (2016), arXiv:1610.03507 [quant-ph].

[7] J. Roffe, D. Headley, N. Chancellor, D. Horsman, and V. Kendon, Protecting quantum memories using coherent parity check codes, *Quantum Science and Technology* **3**, 035010 (2018).

[8] N. M. Linke, M. Gutierrez, K. A. Landsman, C. Figgatt, S. Debnath, K. R. Brown, and C. Monroe, Fault-tolerant quantum error detection, *Science Advances* **3**, 10 (2017).

[9] R. Harper and S. T. Flammia, Fault-tolerant logical gates in the IBM quantum experience, *Physical Review Letters* **122**, 8 (2019).

[10] C. Vuillot, Is error detection helpful on IBM 5Q chips?, *Quantum Information and Computation* **18**, 0949 (2018).

[11] E. Knill, Quantum computing with realistically noisy devices, *Nature* **434**, 39–44 (2005).

[12] A. Gonzales, D. Dilley, B. Li, L. Jiang, and Z. H. Saleem, Detecting errors in a quantum network with Pauli checks, *Physical Review A* **111**, 052629 (2025).

[13] N. Isailovic, Y. Patel, M. Whitney, and J. Kubiatowicz, Interconnection networks for scalable quantum computers, in *33rd*

International Symposium on Computer Architecture (ISCA '06) (2006) pp. 366–377.

[14] O. Boncalo and A. Amaricai, Reliability analysis of qubit data movement for distributed quantum computation, in *2009 12th Euromicro Conference on Digital System Design, Architectures, Methods and Tools* (2009) pp. 481–487.

[15] V. Siddhu, E. Winston, D. C. McKay, and A. Javadi-Abhari, Basic distillation with realistic noise (2025), arXiv:2504.06175 [quant-ph].

[16] C. H. Bennett, G. Brassard, C. Crépeau, R. Jozsa, A. Peres, and W. K. Wootters, Teleporting an unknown quantum state via dual classical and Einstein-Podolsky-Rosen channels, *Physical Review Letters* **70**, 1895 (1993).

[17] D. Bouwmeester, J.-W. Pan, K. Mattle, M. Eibl, H. Weinfurter, and A. Zeilinger, Experimental quantum teleportation, *Nature* **390**, 575 (1997).

[18] L. Jiang, J. M. Taylor, K. Nemoto, W. J. Munro, R. Van Meter, and M. D. Lukin, Quantum repeater with encoding, *Physical Review A* **79**, 032325 (2009).

[19] D. W. Leung, M. A. Nielsen, I. L. Chuang, and Y. Yamamoto, Approximate quantum error correction can lead to better codes, *Physical Review A* **56**, 2567–2573 (1997).

[20] P. W. Shor, Scheme for reducing decoherence in quantum computer memory, *Physical Review A* **52**, R2493 (1995).

[21] Y. Jing, D. Alsina, and M. Razavi, Quantum key distribution over quantum repeaters with encoding: Using error detection as an effective postselection tool, *Physical Review Applied* **14**, 064037 (2020).

[22] T. Coopmans *et al.*, Netsquid, a discrete-event simulation platform for quantum networks, *Communications Physics* **4**, 164 (2021).

[23] K. Campbell, dqc_simulator, https://github.com/km-campbell/dqc_simulator.git.

[24] H. Briegel, W. Dür, J. Cirac, and P. Zoller, Quantum repeaters: The role of imperfect local operations in quantum communication, *Physical Review Letters* **81**, 5932 (1998).

[25] Ionq aria: Practical performance, <https://ionq.com/resources/ionq-aria-practical-performance> (2023), last accessed: 02/07/2025.

[26] A. Wu, H. Zhang, G. Li, A. Shabani, Y. Xie, and Y. Ding, Autocomm: A framework for enabling efficient communication in distributed quantum programs, in *2022 55th IEEE/ACM International Symposium on Microarchitecture (MICRO)* (2022) pp. 1027–1041.

[27] T. S. Metodi, D. D. Thaker, A. W. Cross, F. T. Chong, and I. L. Chuang, A quantum logic array microarchitecture: Scalable quantum data movement and computation (2005), arXiv:0509051 [quant-ph].

[28] L. J. Stephenson, D. P. Nadlinger, B. C. Nichol, S. An, P. Drmota, T. G. Ballance, K. Thirumalai, J. F. Goodwin, D. M. Lucas, and C. J. Ballance, High-rate, high-fidelity entanglement of qubits across an elementary quantum network, *Physical Review Letters* **124**, 110501 (2020).

[29] R. Paschotta, Fibers, RP Photonics Encyclopedia (2006), available online at <https://www.rp-photonics.com/fibers.html>.

[30] Quantinuum performance validation, https://docs.quantinuum.com/systems/user_guide/hardware_user_guide/performance_validation.html (2025), last accessed: 02/07/2025.